6-1-2018

First-principles study of electronic structure and Fermi surface in semimetallic YAs

Przemyslaw Swatek
Iowa State University and Ames Laboratory, pswatek@ameslab.gov

First-principles study of electronic structure and Fermi surface in semimetallic YAs

Abstract
In the course of searching for new systems, which exhibit nonsaturating and extremely large positive magnetoresistance, electronic structure, Fermi surface, and de Haas-van Alphen characteristics of the semimetallic YAs compound were studied using the all-electron full-potential linearized augmented-plane wave (FP-LAPW) approach in the framework of the generalized gradient approximation (GGA). In the scalar-relativistic calculation, the cubic symmetry splits fivefold degenerate Y-d orbital into low-energy threefold-degenerate t(2g) and twofold degenerate doublet e(1g) states at Gamma point around the Fermi energy. One of them, together with the threefold degenerate t(1u) character of As-p orbital, render the YAs semimetal with a topologically trivial band order and fairly low density of states at the Fermi level. Including spin-orbit (SO) coupling into the calculation leads to pronounced splitting of the t(1u) state and shifting the bands in the energy scale. Consequently, the determined four different 3-dimensional Fermi surface sheets of YAs consists of three concentric hole-like bands at G and one ellipsoidal electron-like sheet centred at the X points. In full accordance with the previous first-principles calculations for isostructural YSb and YBi, the calculated Fermi surface of YAs originates from fairly compensated multi-band electronic structures.

Keywords
Electronic-structure, Fermi surface, Quantum oscillations, Large magnetoresistance, Ab initio calculations

Disciplines
Engineering Physics | Materials Science and Engineering | Metallurgy | Physics

First-principles study of electronic structure and Fermi surface in semimetallic YAs

Przemysław Swatek[a,b,c]

[a] *Institute of Low Temperature and Structure Research, Polish Academy of Sciences, Wrocław, Poland*
[b] *Division of Materials Science and Engineering, Ames Laboratory, Ames, Iowa 50011, USA*
[c] *Department of Physics and Astronomy, Iowa State University, Ames, Iowa 50011, USA*

Abstract

In the course of searching for new systems, which exhibit nonsaturating and extremely large positive magnetoresistance, electronic structure, Fermi surface, and de Haas-van Alphen characteristics of the semimetallic YAs compound were studied using the all-electron full-potential linearized augmented-plane wave (FP–LAPW) approach in the framework of the generalized gradient approximation (GGA). In the scalar-relativistic calculation, the cubic symmetry splits five-fold degenerate Y-d orbital into low-energy threefold-degenerate t_{2g} and two-fold degenerate doublet e_{1g} states at Γ point around the Fermi energy. One of them, together with the three-fold degenerate t_{1u} character of As-p orbital, render the YAs semimetal with a topologically trivial band order and fairly low density of states at the Fermi level. Including spin-orbit (SO) coupling into the calculation leads to pronounced splitting of the t_{1u} state and shifting the bands in the energy scale. Consequently, the determined four different 3-dimensional Fermi surface sheets of YAs consists of three concentric hole-like bands at Γ and one ellipsoidal electron-like sheet centred at the X points. In full accordance with the previous first-principles calculations for isostructural YSb and YBi, the calculated Fermi surface of YAs originates from fairly compensated multi-band electronic structures.

Keywords: Electronic-structure, Fermi surface, Quantum oscillations, Large magnetoresistance, Ab initio calculations.

Introduction

The ability to drastically change electrical resistance in response to a magnetic field is one of the most justifying qualities in modern materials science and engineering. Recent reports of nonsaturating and extremly large positive magnetoresistance in several nonmagnetic and magnetic binary semimetals with the overall composition RX (R = rare-earth; X = p-electron element from Group 15 of the periodic table) have attracted a lot of attention [1, 2, 3, 4]. The interesting properties of transition-metal monophosphides motivate us examine other rare-earth arsenides with the same crystal structure.

Email address: P.Swatek@int.pan.wroc.pl (Przemysław Swatek)

Despite a growing number of new materials, which exhibit extreme magnetoresistance effect (XMR), the underlying mechanisms of this effect remains debate.

YAs is isostructural and isovalent to YSb. Both compounds crystallize with a simple cubic cell (space group $Fm\bar{3}m$, No. 225), in the NaCl type. The lattice parameter a = 5.798 Å reported for YAs is slightly smaller than that of YSb (a = 6.1652 Å) [5, 6, 7], reflecting smaller size of the As ion. YSb is a typical example of monopnictides exhibiting nonsaturating large magnetoresistance $MR \sim 10^5\%$ in a field of 9 T at low temperatures [19]. MR varies with B quadratically in weak fields and almost linearly in strong fields, in a manner observed in many semimetallic materials, such as (Nb,Ta)As, (Nb,Mo,Ta)As_2, (Pd,Pt)Sn_4 or WTe_2 [8, 9, 10, 12, 11, 13, 14, 15].

Recently, a few mechanisms have been suggested as the origin of XMR in nomagnetic YSb: (i) nearly perfect electron-hole compensation[16, 17] (ii) moderate carrier compensation with substantial mobility difference[18] (iii) $d - p$ orbital mixing combined with carrier compensation[19] (iv) magnetic field induced metal-insulator-like transition [5]. While electrical transport properties fairly similar to those of YSb have been reported for the bismuthide YBi [5, 17, 18, 19, 20], no such data are available in the literature for the arsenide YAs. As regards the electronic structure of YAs, some calculations were made at a scalar relativistic level [21, 22, 23, 24], yet full description of the Fermi surface is lacking.

The aim of this work was to investigate the electronic structure and the Fermi surface of YAs by means of the first principle calculations.

Method of calculations

Electronic structure calculations were performed with the all-electron general potential linearized augmented plane-wave method as implemented in the Wien2k code [25]. The exchange and correlation effects were treated using GGA in the form proposed by Perdew, Wang and Ernzerhof [26]. SO coupling was included as a second variational step, using scalar-relativistic eigenfunctions as the basis, after the initial calculation was converged to self-consistency. The Monkhorst–Pack special k-point scheme with $46 \times 46 \times 46$ mesh was used in the first Brillouin zone sampling, and the cutoff parameter ($R_{mt}K_{max}$) was set to 8. For the Fermi surface, the irreducible Brillouin zone was sampled by 20225 k points to ensure accurate determination of the Fermi level [27]. De Haas–van Alphen (dHA) frequencies were calculated using the Supercell K-space Extremal Area Finder tool [28].

For the reference data of DOS similar calculations were performed with a full potential all-electron local orbital code FPLO-9.00-34 [29, 30], using the same type of the exchange-correlation potential as above. In both calculations, the experimental lattice parameter a = 5.798 Å of YAs was assumed [6, 7].

Results and discussion

Electronic structure calculations

Figure 1 presents the total density of states (DOS) of YAs calculated using the FP-LAPW and FPLO methods. In the Wien2k calculation spin-orbit coupling was included

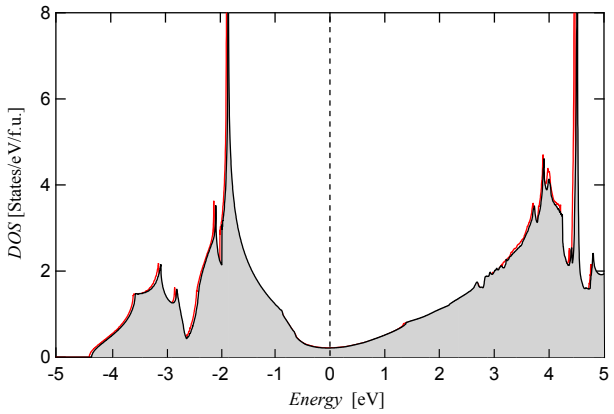

Figure 1: (Color online) Comparison of DOS plots obtained from the full-relativistic FPLO (thin gray) and FP–LAPW with SO (thick red) calculations to show the equivalence of both methods for YAs.

in the second variational step, whereas in FPLO-9.00-34 code the full 4-component Kohn-Sham-Dirac equation, containing implicitly SO coupling up to all orders, was solved self-consistently. The results are independent of the approach, establishing that the different treatment of relativistic and correlation effects in both codes yield reliable picture of the electronic structure of YAs. Therefore, in the following only the data obtained by FP–LAPW are discussed.

The Fermi energy (E_F) of YAs locates between two large separated features at wide valley of DOS. The Sommerfeld coefficient in the specific heat can be estimated from the DOS data using $\gamma = (\pi^2/3)N(E_F k_B^2)$ where k_B is the Boltzmann constant and $N(E_F)$ is the density of states at the Fermi energy. The so-obtained $\gamma = 0.51$ mJ/mol K^2 is slightly smaller than the experimental value of 0.9 mJ/mol K^2, yet similar to the value $\gamma = 0.45$ mJ/mol K^2 calculated for YSb and YSe [31, 32, 33].

To determine the influence of SO coupling on the electronic structure of YAs, calculations of energy band dispersions were carried out in the first step at the scalar relativistic level. If one compares the previously calculated band structures of YAs and YSb [5, 34], one finds that in both cases the overall dispersion is very similar, with four bands crossing the Fermi level: three-fold degenerate hole-like bands pinned at about 0.4 eV above E_F at the Γ point and one elongated electron band close to the X-point at the border of the Brillouin zone (BZ).

Additionally, by calculating different band characters, one can see that the bands near E_F are dominated by contributions from p states of As, whereas Y-d states are mostly unfilled. In crystalline field potential of O_h symmetry five d-orbitals split into three orbitals with t_{2g} (d_{xz}, d_{yz}, d_{xy}) character and two orbitals with e_g (d_{z^2}, $d_{x^2y^2}$) character. One d-band from the t_{1u} manifold, drops dramatically and dips below E_F as one moves along $\Gamma - X$ direction and then rapidly rises along $X - Z - W$ path. In turn, 3-fold degenerate p orbital with t_{1u} character located at the Γ point is not affected by surrounding interaction. Two $p_{x,y}$ orbitals are doubly degenerated along X-Γ-L path, whereas p_z is clearly separated from the others in the other part of BZ.

As can be inferred from Fig. 2b, inclusion of SO coupling into the calculations

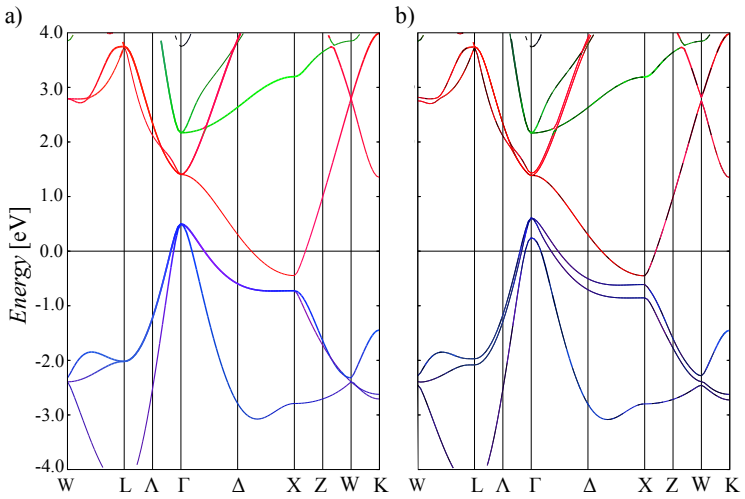

Figure 2: (Color online) Energy bands dispersion in YAs calculated using scalar relativistic FP–LAPW method without (a) and with (b) inclusion of SO coupling. The amounts of Y-d and As-p characters are indicated by the colors of the bands; green symbols denote Y-d – e_g, red Y-d – t_{2g}, and blue As-5p, respectively.

induces a lifting/lowering of the degeneracy of p-states. The whole p_z-band shifts toward lower binding energy, thus only a small part of the band persists above E_F at Γ point. In turn, two highest-energy As-$p_{x,y}$ bands become noticeably separated from each other along Γ-X path. Similar rearrangement of these two p-bands can also be seen along L-Γ direction, however, the influence of SO coupling in this case is less noticeable. Finally, comparing our data to the earlier calculations [4, 16, 19, 20, 33], the size of the SO splitting of the p bands increases on going from YAs to YSb to YBi, in line with general expectation.

At the X point at 0.5 eV below the Fermi level, a gap of about 160 meV appears between p and d bands. It is twice larger than the gap derived for YSb in fully relativistic FPLO calculations with GGA [19]. Remarkably, no topological band inversion is recognized for YAs, which indicates the absence of any topologically non-trivial electronic states. It is worth recalling that a similar conclusion was recently formulated for YSb, based on angle-resolved photoemission spectroscopy (ARPES) data and angle-dependent Shubnikov de Haas experiments, which were supported by first principles calculations [4, 16, 18, 19].

Figure 3 shows the calculated Fermi surfaces in YAs. Moreover, there are depicted (101)-angular dependencies of the Fermi surface pockets cross-sectional areas. The 3-dimensional Fermi surface consists of three nested hole-like and one electron-like sheets at the Γ and X points, respectively. The smallest innermost sheet, labeled ζ, is perfectly circular. Remarkably, its orbital character, as inferred from the GGA calculations, is p_z; i.e., it belongs to the t_{1u} manifold, which is fully occupied in YBi [20]. The larger square-shaped octahedron β and cross-shaped δ sheet with pronounced uniaxial anisotropy derive from the out-of-plane $p_{x,y}$ orbitals. Around the X points, an

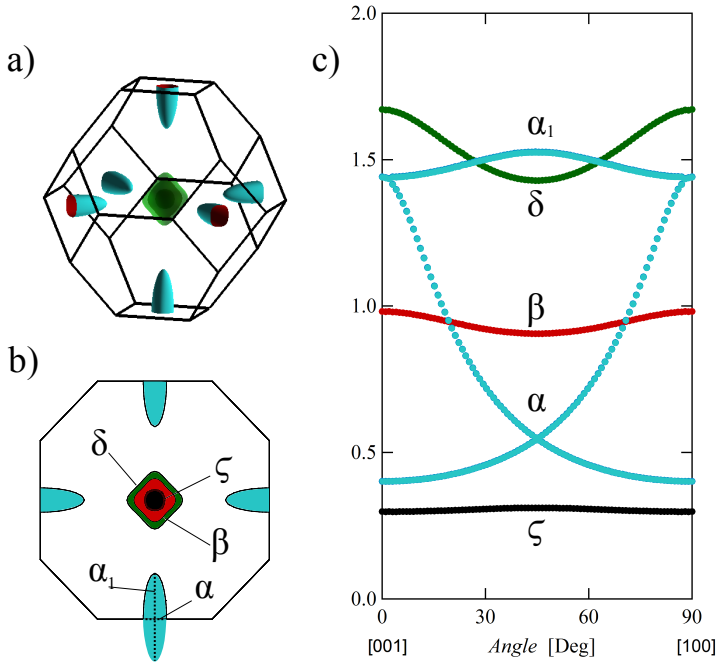

Figure 3: (Color online) (a) Fermi surface (b) sketch through the Brillouin zone of a (001) of YAs calculated in this work using FP–LAPW method with spin-orbin coupling. Triplicate electron pocket and three hole pockets labeled α, β, δ and ζ. (c) The corresponding (110)-plane angle evolution of the cross-sectional areas (in frequency units) of the calculated Fermi surface pockets.

electron-like prolate ellipsoid α with mostly d_{xy} orbital character can be identified.

The calculated volume $V_F^h \approx 0.0622$ Å^3 enclosed by three hole-like pockets is approximately equal to the volume of the electron pocket ($V_F^e \approx 0.0624$ Å^3), yielding $V_F^h/V_F^e \approx 0.997$. Recently, it was shown that applying the modified Tran and Blaha Becke-Johnson potential [35] improves the agreement between the ARPES data and the results of band structure calculations made for YSb [18]. In the case of YAs, the latter approach yields shrinking all the Fermi surface sheets (not shown), however the ratio $V^h_{F\_mBJ}/V^e_{F\_mBJ} \approx 0.994$ remains nearly constant. This finding suggests that YAs is another highly compensated semimetal, alike other non-magnetic representatives of the *RX* family [4, 19, 20, 36, 37, 38, 39, 40, 41].

Conclusions

We have performed first-principle calculations of the density of states and the energy band structure of YAs. Our investigation of this system was motivated by the presumed similarity of the transport characteristics of this material to those of the isostructural antimonide YSb, which was recently reported to exhibit nonsaturating extremely large magnetoresistance and high mobility of charge carriers [16, 17, 18, 19].

The SO interaction in YAs was found to be strong enough to lift the three-fold degeneracy of the As-p state at the Γ point. With one electron-like Y-d orbital and three

different As-p hole-like 3-dimensional Fermi surface sheets, YAs seems to be a nearly compensated semimetal with topologically trivial electronic structure. Derived from the topology of the Fermi surface sheets angle resolved quantum oscillations are similar to those recently found in the dHvA experiments on YSb [17, 19]. Since YAs and YSb are isostructural and isoelectronic, one can expect that the primary difference between the two compounds is the SO coupling strength and Pauling electronegativity [42].

Based on the electronic structure data calculated for YAs, one can expect nontrivial transport behavior in this material, namely very large magnetoresistance that does not saturate in strong magnetic fields. Experimental verification of this prediction is wanted.

Data availability

The datasets analysed during the current study are available from the corresponding author on reasonable request.

Acknowledgements

The author thanks Dariusz Kaczorowski, Adam Kaminski, Benjamin Schrunk and Yun Wu for fruitful discussions. The calculations were carried out at the WrocÅaw Centre for Networking and Supercomputing, Grant No. 359. Work at Ames Laboratory was supported by the U.S. Department of Energy, Office of Science, Basic Energy Sciences, Materials Science and Engineering Division. Ames Laboratory is operated for the U.S. Department of Energy by Iowa State University under contract No. DE-AC02-07CH11358.

[1] Tafti, F. F., Gibson, Q. D., Kushwaha, S. K., Haldolaarachchige, N. & Cava, R. J. Resistivity plateau and extreme magnetoresistance in LaSb. *Nat. Phys.* **12**, 272 (2016).

[2] Wu, Y. *et al.* Asymmetric mass acquisition in LaBi: Topological semimetal candidate. *Phys. Rev. B* **94**, 081108(R) (2016).

[3] Tafti, F. F. *et al.* Temperature-field phase diagram of extreme magnetoresistance. *Proc. Natl. Acad. Sci.* **113**, E3475 (2016).

[4] Wu, Y. *et al.* Electronic structure of RSb (R = Y, Ce, Gd, Dy, Ho, Tm, Lu) studied by angle-resolved photoemission spectroscopy. *Phys. Rev. B* **96**, 035134 (2017).

[5] Ghimire, N. J., Botana, A. S., Phelan, D., Zheng, H. & Mitchell, J. F. Magnetotransport of single crystalline YSb. *J. Phys. Condens. Matter* **28**, 235601 (2016).

[6] Palewski, T. The Magnetic Properties of $U_xY_{1x}As$ Solid Solution. *Phys. Stat. Sol. A: Applied Research* **88**, K149 (1985).

[7] Faktor M.M., Hanks R. Calculation of the third ionisation potentials of the lanthanons. *J. Inorg. Nuc. Chem* **31**, 1649 (1969).

[8] Xu, S.Y. *et al.* Discovery of a Weyl fermion state with Fermi arcs in niobium arsenide. *Nat. Phys.* **11**, 748 (2015).

[9] Huang, X. *et al.* Observation of the Chiral-Anomaly-Induced Negative Magnetoresistance in 3D Weyl Semimetal TaAs. *Phys. Rev. X* **5**, 031023 (2015).

[10] Shen, B. *et al.* Fermi surface topology and negative longitudinal magnetoresistance observed in the semimetal $NbAs_2$. *Phys. Rev. B* **93**, 195119 (2016).

[11] Wang, Y. Y. *et al.* Resistivity plateau and extremely large magnetoresistance in $NbAs_2$ and $TaAs_2$. *Phys. Rev. B* **94**, 041103 (2016).

[12] Lou, R. *et al.* Observation of open-orbit Fermi surface topology in the extremely large magnetoresistance semimetal $MoAs_2$. *Phys. Rev. B* **24**, 241106 (2017).

[13] Jo, N. H. *et al.* Extremely large magnetoresistance and Kohlers rule in PdSn4: A complete study of thermodynamic, transport, and band-structure properties. *Phys. Rev. B* **96**, 165145 (2017)

[14] Mun, E. *et al.* Magnetic field effects on transport properties of $PtSn_4$. *Phys. Rev. B* **95**, 035135 (2012)

[15] Jiang, J. *et al.* Signature of strong spin-orbital coupling in the large nonsaturating magnetoresistance material WTe_2. *Phys. Rev. Lett.* **115**, 166601 (2015).

[16] Xu, J. *et al.* Origin of the extremely large magnetoresistance in the semimetal YSb. *Phys. Rev. B* **96**, 075159 (2017).

[17] Yu, Q. *et al.* Magnetoresistance and Shubnikov-de Haas oscillation in YSb. *EPL Europhysics Lett.* **119**, 1 (2017).

[18] He, J. *et al.* Distinct electronic structure for the extreme magnetoresistance in YSb. *Phys. Rev. Lett.* **117**, 267201 (2016).

[19] Pavlosiuk, O., Swatek, P. & Wiśniewski, P. Giant magnetoresistance, three-dimensional Fermi surface and origin of resistivity plateau in YSb semimetal. *Sci. Rep.* **6**, 38691 (2016).

[20] Pavlosiuk, O., Swatek, P., Kaczorowski, D. & Wiśniewski, P. Magnetoresistance in YBi and LuBi semimetals due to nearly perfect carrier compensation. *arXiv preprint no.* 1712.08433 (2017).

[21] Said, M. *et al.* First-principles electronic structure of rare-earth arsenides. *Eur. Phys. J. B* **23**, 191 (2001).

[22] Amrani, B. El Haj Hassan, F. Theoretical study of IIIV yttrium compounds. *Computational Materials Science* **39**, 563 (2007).

[23] Bouhemadou, A. Elastic constants and high pressure structural transitions in yttrium pnictides. *Computational Materials Science* **43**, 1112 (2008).

[24] Yassine, Ch.Loutfi, B. First-Principles Calculations of the Dynamical and Thermodynamic Properties of Yttrium Compounds YX (X = N, P, As and Sb). *J. Phase Equilib. Diffus.* **37**, 336 (2016).

[25] Blaha, P., Schwarz, K., Madsen, G. K. H., Kvasnicka, D. & Luitz, J. *WIEN2K, an augmented plane wave + local orbitals program for calculating crystal properties* (Technische Universität Wien,2001).

[26] Perdew, J. P., Burke, K. & Ernzerhof, M. Generalized gradient approximation made simple. *Phys. Rev. Lett.* **77**, 3865 (1996).

[27] Kokalj, A. Computer graphics and graphical user interfaces as tools in simulations of matter at the atomic scale. *Comput. Mater. Sci.* **28**, 155 (2003).

[28] Rourke, P. M. C. & Julian, S. Numerical extraction of de Haas-van Alphen frequencies from calculated band energies. *Comput. Phys. Commun.* **183**, 324 (2012).

[29] Koepernik, K. & Eschrig, H. Full-potential nonorthogonal local-orbital minimum-basis band-structure scheme. *Phys. Rev. B* **59**, 1743 (1999).

[30] Koepernik, K., Velicky, B, Hayn, R & Eschrig, H. Self-consistent LCAO-CPA method for disordered alloys. *Phys. Rev. B* **55**, 5717 (1997).

[31] Gambino, R. , Eastman, D., McGuire, T., Moruzzi, V. & Grobman, W. Evidence of the Intrinsic Metallic Character of Some RareEarth Pnictides. *J. Appl. Phys.* **42**, 1468 (1971).

[32] Seddik, T. *et al.* Prediction study of the structural, elastic and high pressure properties of Yttrium chalcogenide. *Comput. Mater. Sci* **49**, 372 (2010).

[33] Larson, P. Electronic structure of rare-earth nickel pnictides: Narrow-gap thermoelectric materials. *Phys. Rev. B* **59**, 15660 (1999).

[34] Pagare, G., Chouhan, S. S., Soni, P., Sanyal, S. P. & Rajagopalan, M. First principles study of structural, electronic and elastic properties of lutetium monopnictides. *Comput. Mater. Sci.* **50**, 538 (2010).

[35] Tran, F. & Blaha, P. Accurate band gaps of semiconductors and insulators with a semilocal exchange-correlation potential. *Phys. Rev. Lett.* **102**, 226401 (2009).

[36] Pavlosiuk, O., Kleinert, M., Swatek, P., Kaczorowski, D., & Wiśniewski, P. Fermi surface topology and magnetotransport in semimetallic LuSb. *Sci. Rep.* **7**, 12822 (2017).

[37] Żogał, O., Wawryk, R., Matusiak, M. & Henkie, Z. Electron transport and magnetic properties of semimetallic LuAs. *J. Alloys Compd.* **587**, 190 (2014).

[38] Yang, H.-Y. *et al.* Extreme magnetoresistance in the topologically trivial lanthanum monopnictide LaAs. *Phys. Rev. B* **96**, 235128 (2017).

[39] Juraszek, J. *et al.* Extreme magnetoresistance in the regular semimetal LuAs. Poster session presented at The European Conference Physics of Magnetism 2017 (PM17), Poznan (2017).

[40] Sun, S. *et al.* Large magnetoresistance in LaBi: origin of field-induced resistivity upturn and plateau in compensated semimetals. *New J. Phys* **18**, 082002 (2016).

[41] Niu, N. H. *et al.* Presence of exotic electronic surface states in LaBi and LaSb. *Phys. Rev. B* **94**, 165163 (2016).

[42] Cao, G. *et al.* A simple and efficient criterion for ready screening of potential topological insulators. *Sci. Bull* **62**, 1649 (2017).